

Time multiscale modeling of sorption kinetics I: uniformly accurate schemes for highly oscillatory advection-diffusion equation

Clarissa Astuto¹, Mohammed Lemou², and Giovanni Russo³

¹King Abdullah University of Science and Technology (KAUST), 4700, Thuwal, Saudi Arabia

²IRMAR, CNRS et Université de Rennes 1, France

³Department of Mathematics, University of Catania, Italy

July 27, 2023

Abstract

In this paper we propose a numerical method to solve a 2D advection-diffusion equation, in the highly oscillatory regime. We use an efficient and robust integrator which leads to an accurate approximation of the solution without any time step-size restriction. Uniform first and second order numerical approximations in time are obtained with errors, and at a cost, that are independent of the oscillation frequency. This work is part of a long time project, and the final goal is the resolution of a Stokes-advection-diffusion system, in which the expression for the velocity in the advection term, is the solution of the Stokes equations. This paper focuses on the time multiscale challenge, coming from the velocity that is an ε -periodic function, whose expression is explicitly known. We also introduce a two-scale formulation, as a first step to the numerical resolution of the complete oscillatory Stokes-advection-diffusion system, that is currently under investigation. This two-scale formulation is also useful to understand the asymptotic behaviour of the solution.

1 Introduction

The diffusion of particles, in presence of moving traps, is an interesting topic in different areas, from biology [20, 16, 19, 27] to chemistry [3, 22], with a relevant application to the study of the relation between living cell membranes and substances freely diffusing around them [25, 15, 14].

With the aim of studying the capture rate (chemoreception), a biomimetic model has been developed [28, 29, 25], in which an oscillating air bubble mimics a fluctuating cell, and a flow of charged surfactants simulates the diffusing substances (see Fig. 1 (a)). Surfactants are composed by anions and cations, that have two different configurations. The cations

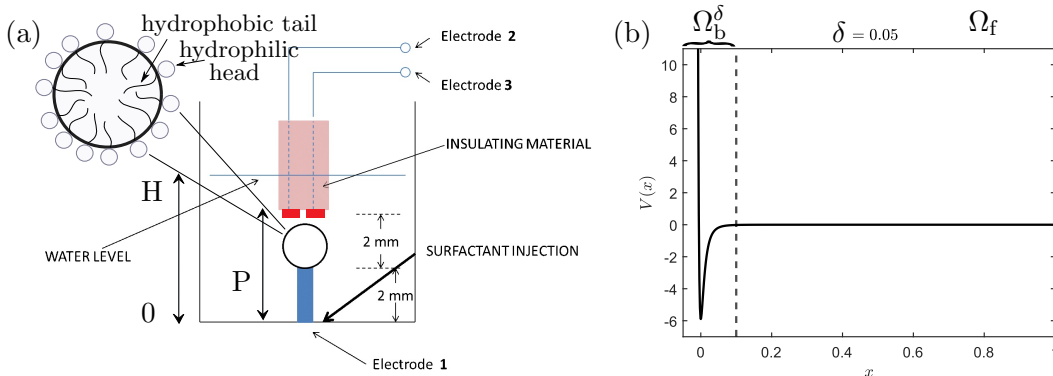


Figure 1: (a): *Scheme of the experimental setup.* On the top left there is a zoom in of the anions behaviour at the air-surface of the bubble, with the hydrophobic tails inside the air bubble, and the hydrophilic heads on the surface. The water level is H and the detector is located in a point P . (b) *Scheme of the potential $V(x)$, defined in Eq. (3), where δ is the thickness of the attractive-repulsive part.*

are hydrophilic, while the negative ions have both hydrophilic and hydrophobic parts, and, for this reason, they are absorbed at the air-water interface (see Fig. 1 (a)).

The problem of surfactant diffusion or molecules, that are adsorbed at the surface of a moving cell, has been investigated by several authors [25, 2, 24, 17, 18, 26, 4, 30] and the starting model for the evolution of a single species carriers is the one described in [2], where the authors introduced the local concentration of ions¹ $c = c(\vec{x}, t)$, whose time evolution in a static fluid is governed by the conservation law

$$\frac{\partial c}{\partial t} = -\nabla \cdot J. \quad (1)$$

In presence of a static bubble (see Fig. 1 (a)), and for small concentrations c , the flux has the following expression

$$J = -D \left(\nabla c + \frac{1}{k_B T} c \nabla V \right) \quad (2)$$

where D is the diffusion coefficient, k_B is the Boltzmann's constant, T is the absolute temperature and V is a suitable potential function that describes the *attractive-repulsive* behavior of the bubble with the particles (see Fig. 1 (b)).

For simplicity, here we describe only the one space dimension model (see [2] for more details and dimensions). We assume that the fluid domain, which is not affected by the bubble, is $\Omega_f^\delta = [L\delta, 1]$, and that the attractive-repulsive mechanism of the bubble is simulated inside

¹In reality there are two types of ions, anions and cations, each with its own concentration, mutually attracting each other by Coulomb interaction. In the so called quasi-neutral limit the two concentrations completely overlap, and the system can be described by just one scalar concentration, see [2].

a thin region $\Omega_b^\delta = [-\delta, L\delta]$, with L a constant of order 1. It means that the potential $V(x) = 0$ for $x \in \Omega_f^\delta$.

In particular, the particles, that are close to the bubble, are attracted by its surface, but, at the same time, when an attracted particle is at very short distance from the surface of the bubble, it is repulsed, so that it cannot enter inside the bubble. This repulsion simulates the impermeability of the air bubble, and, in [2] we choose the Lennard-Jones potential (LJ) as a prototypical attractive-repulsive potential, as follows

$$V(x) = E \left(\left(\frac{x + \delta}{\delta} \right)^{-12} - 2 \left(\frac{x + \delta}{\delta} \right)^{-6} \right), \quad (3)$$

where δ denotes the range of the potential and E represents the depth of the well, (see Fig. 1 (b)).

In [2] we proposed a *multiscale model*, based on asymptotic expansion in δ , to describe this adsorption-desorption behaviour. The space multiscale nature derives from the potential that is not negligible only in Ω_b^δ , which is very small compared to the entire domain.

Summarizing, the 1D multiscale model for a single carrier, in the low concentration approximation, can be obtained for $\delta \ll 1$ (in general, for $\delta/L_x \ll 1$ where L_x is the length of the 1D domain) as follows:

$$\frac{\partial c}{\partial t} = D \frac{\partial^2 c}{\partial x^2} \quad \text{in } x \in [0, 1] \quad (4)$$

$$\frac{\partial c}{\partial x} = 0 \quad \text{at } x = 1, \quad \mathcal{M} \frac{\partial c}{\partial t} = D \frac{\partial c}{\partial x} \quad \text{at } x = 0 \quad (5)$$

and

$$\mathcal{M} = \delta \int_0^{L+1} \exp(-U(\zeta)) d\zeta. \quad (6)$$

where $U(\zeta) = \phi (\zeta^{-12} - 2\zeta^{-6})$ is a non dimensional form of the potential $V(x)$, with $\zeta = 1 + x/\delta \in [0, L + 1]$ is a rescaled variable, L is the distance at which the potential U is negligible and $\phi = E/k_B T$. In our case, we pose $L = 2$.

In this scenario, it is important the role played by oscillating traps with particles, as well as, the computation of their adsorption and desorption rates at the surface of the trap. In [1], we add an advection term to the diffusion equation, to take into account the movement of the fluid, due to the oscillations of the bubble. Then we couple the advection-diffusion equation for the particle concentration, with the Stokes equations for the fluid velocity, and we consider different kinds of oscillations, e.g., radial oscillations or shape deformations, where we show how the diffusion rate depends on the type of oscillations and on its frequency.

In this work, we focus on the time multiple scale nature of the problem. The technique we use is based on the assumption that the motion of the bubble, and the fluid, are periodic in time, with a period ε that is much shorter than typical diffusion times. Indeed, in laboratory

experiments, bubble oscillations frequency is of the order of hundred Hz, while the diffusing time is of the order of hours (see [25, 24] for more details).

Standard numerical methods, for the Eq. (9), produce errors of the order $\Delta t^p/\varepsilon^q$, for some positive p and q . In that way, the user is forced to obey to the restriction on the time step to obtain the desired accuracy, i.e., $\Delta t \lesssim \varepsilon^{q/p}$. This restriction becomes prohibitive for small values of ε . We will follow the strategy adopted in [5, 6, 7, 12, 13] although in the different contexts of Vlasov–Poisson equations, Klein–Gordon and nonlinear Schrödinger equations, to obtain a robust scheme that is able to deal with a large range of $\varepsilon \in (0, 1]$ (being small or not), since our goal is to obtain a numerical scheme that is uniformly accurate in ε .

2 Model

In this paper we investigate the time multiscale coming from the advection term in the system. As a preliminary, work we assume that the expression for the velocity is known, and we do not have to compute the solution of the Stokes equations.

In the presence of a moving fluid, the conservation law for the local concentration of ions $c = c(\vec{x}, t)$ is the same as (1)

$$\frac{\partial c}{\partial t} = -\nabla \cdot \vec{J}, \quad \text{in } \mathcal{S}, \quad (7)$$

where $\mathcal{S} \subset \mathbb{R}^2$. However, this time the flux term \vec{J} contains a diffusion and an advection term,

$$\vec{J} = -D\nabla c - c\vec{u}, \quad t \in [0, t_{\text{fin}}] \quad (8)$$

where $t_{\text{fin}} > 0$, D is the diffusion coefficient, $\vec{u} = \vec{u}(\vec{x}, t/\varepsilon) \in \mathbb{R}^2$ is explicitly known in space and time, and is assumed to be a periodic vector function of time with period equal to $\varepsilon \in]0, \varepsilon_0]$, for some $\varepsilon_0 > 0$. We add a subscript ε on the concentration $c_\varepsilon = c$, to emphasize its dependence on the oscillation period, and at the end, the system reads

$$\frac{\partial c_\varepsilon}{\partial t} = D\Delta c_\varepsilon + \nabla \cdot (c_\varepsilon \vec{u}(t/\varepsilon)), \quad \text{in } \mathcal{S}. \quad (9)$$

From now on, we omit to indicate the explicit dependence of \vec{u} on space, while we keep its dependence on t/ε . Let \mathcal{S} be a square, and $\Omega = \mathcal{S} \setminus \mathcal{B}$ the computational domain where \mathcal{B} is a circle centered in $(0, 0)$, with radius $R_{\mathcal{B}}$ (see Fig. 2 (a)). The boundary of the domain is defined as $\Gamma = \partial\Omega = \Gamma_{\mathcal{S}} \cup \Gamma_{\mathcal{B}}$; see Fig. 2 (a).

Eq. (9) is completed with homogeneous Neumann boundary conditions in $\Gamma_{\mathcal{S}}$ and absorption-desorption boundary conditions in $\Gamma_{\mathcal{B}}$ (see [2] for more details), i.e., in other words

$$\nabla c_\varepsilon \cdot n = 0 \quad \text{on } \Gamma_{\mathcal{S}} \quad (10)$$

$$\mathcal{M} \frac{\partial c_\varepsilon}{\partial t} = \mathcal{M} D \frac{\partial^2 c_\varepsilon}{\partial \tau^2} - D \frac{\partial c_\varepsilon}{\partial n} \quad \text{on } \Gamma_{\mathcal{B}}, \quad (11)$$

where n is the outgoing normal vector to Γ , and τ is the tangent vector to $\Gamma_{\mathcal{B}}$. Eq. (11) is the analogue expression of Eq. (6), but in higher dimension.

To close the system (9-11), we add an initial condition

$$c_\varepsilon(0) = c_\varepsilon^0 \quad (12)$$

that does not depend on ε .

Considering a numerical scheme of order $q > 1$, it means by definition that for all $\varepsilon > 0$, there exists a constant $K(\varepsilon)$, and a time-step $\overline{\Delta t}(\varepsilon)$ such that, for all $\Delta t < \overline{\Delta t}(\varepsilon)$, the error $E_\varepsilon(\Delta t)$ is bounded by

$$E_\varepsilon(\Delta t) < K(\varepsilon)\Delta t^q. \quad (13)$$

The goal of this paper is to construct numerical schemes that are stable, for all $\varepsilon \in (0, 1]$, and whose order does not depend on ε and does not degrade when $\varepsilon \rightarrow 0$. In other word, there exist a constant K , independent of ε , and a time-step $\overline{\Delta t}$ such that, for all $\Delta t < \overline{\Delta t}$, the error $E(\Delta t)$ is bounded by

$$E(\Delta t) < K\Delta t^q,$$

where q is the same as in Eq. (13).

To show that the numerical schemes, proposed in this paper, are uniformly accurate in ε , we first observe that there are not oscillations of lengthscale proportional to ε in space.

Remark 1. *Since $\vec{u}(t/\varepsilon)$ depends on \vec{x} but not on \vec{x}/ε , the solution c_ε is not oscillatory in space. This is attested by numerical tests, see Figs. 7. However, if u oscillates in \vec{x} (which means that it has some smooth dependence on \vec{x}/ε), then the solution c_ε is oscillating in space as well. This is also observed in Fig. 10.*

3 Description of the spatial domain

In this section, we describe the space discretization for Eqs. (9-12). This numerical scheme in space provides a second order accurate method. For more details and accuracy tests about the coupling of the advection-diffusion equation with the Stokes equations see [1], while, for a detailed description of the Navier-Stokes equations in arbitrary moving domains, see [9].

The domain is $\Omega = ([-L_x/2, L_x/2] \times [-L_y/2, L_y/2]) \setminus \mathcal{B}$, with \mathcal{B} a circle centered in $(0, 0)$ and radius $R_{\mathcal{B}}$ (see Fig. 2), and the problem reads:

$$\begin{cases} \frac{\partial c_\varepsilon}{\partial t} = D\Delta c_\varepsilon + \nabla \cdot (c_\varepsilon \vec{u}(t/\varepsilon)) & \text{in } \Omega \\ \nabla c_\varepsilon \cdot n = 0 & \text{on } \Gamma_{\mathcal{S}} \\ \mathcal{M} \frac{\partial c_\varepsilon}{\partial t} = \mathcal{M} D \Delta_{\perp} c_\varepsilon - D \frac{\partial c_\varepsilon}{\partial n} & \text{on } \Gamma_{\mathcal{B}} \end{cases}$$

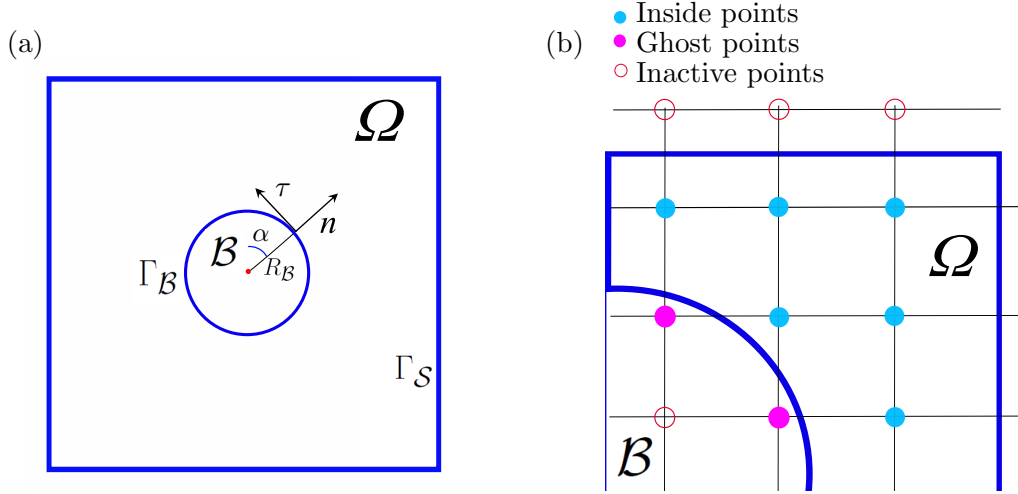


Figure 2: (a): Representation of the domain Ω , where Γ_S is the external wall, while \mathcal{B} is the bubble with boundary Γ_B and radius R_B . The dashed line represents the axis of specular symmetry in 2D and of rotation symmetry in 3D. (b): Classification of the inside (light blue circles), ghost (pink circles) and inactive (red hole circles) points.

where the expression for the velocity $\vec{u}(t/\varepsilon) = \vec{u}(x, y, t/\varepsilon)$ is known, n is the outgoing normal vector to Γ_B , and $\Delta_{\perp} = \partial^2/\partial\tau^2$ denotes the Laplace-Beltrami operator on the circumference of the circle (see Fig. 2)²

3.1 Space discretization

We use a uniform square Cartesian cell-centered discretization, with $\Delta x = \Delta y = h$, and the set of grid points is $\mathcal{S}_h = (x_h, y_h) = \{(x_i, y_j) = (-h/2 + ih, -h/2 + jh), (i, j) \in \{1, \dots, N\}^2\}$, where $N \in \mathbb{N}$ and $h = L_x/N$ with $L_x = L_y = 2$. Here we define the set of internal points $\Omega_h = \mathcal{S}_h \cap \Omega$, the set of bubble points $\mathcal{B}_h = \mathcal{S}_h \cap \mathcal{B}$ and the set of ghost points \mathcal{G}_h , which are bubble points with at least an internal point as neighbor, and are formally defines as follows

$$(x_i, y_j) \in \mathcal{G}_h \iff (x_i, y_j) \in \mathcal{B}_h \text{ and } \{(x_i \pm h, y_j), (x_i, y_j \pm h)\} \cap \Omega_h \neq \emptyset. \quad (14)$$

The other grid points, $\mathcal{S}_h \setminus (\Omega_h \cup \mathcal{G}_h)$, are called inactive points. See Fig. 2 (b) for a classification of inside, ghost, and inactive points. Let $N_I = |\Omega_h|$ and $N_G = |\mathcal{G}_h|$ be the

²This is the same operator that we adopted in [1] when working in the 3D axisymmetric case. We remark here that the exact operator in that case is

$$\Delta_{\perp} = \frac{1}{\sin \alpha} \frac{\partial}{\partial \tau} \left(\sin \alpha \frac{\partial}{\partial \tau} \right)$$

where α is displayed in Fig. 2 (a), and the dashed line represents the axis of specular symmetry in 2D and rotation symmetry in 3D.

cardinality of the sets Ω_h and \mathcal{G}_h , respectively, and $\mathcal{N} = N_I + N_G$ the total number of active points. We compute the solution $c_{\varepsilon,h}$ at the grid points of $\Omega_h \cup \mathcal{G}_h$, by using finite difference discretization of the equations on the N_I internal grid points, and by suitable interpolation to define the conditions for the N_G ghost values. Since each condition on a ghost point may involve other ghost points, the conditions on the ghost points are coupled. For this reason, the whole $\mathcal{N} \times \mathcal{N}$ system, with non-eliminated boundary conditions, is considered.

Representing $c_\varepsilon, c_\varepsilon^0$ and $\vec{u}(t/\varepsilon)$ as column vectors $c_{\varepsilon,h} = (\dots, c_{i,j}^\varepsilon, \dots)^\top, c_{\varepsilon,h}^0 = (\dots, c_{i,j}^{0,\varepsilon}, \dots)^\top, \vec{u}_h(t/\varepsilon) = (\dots, \vec{u}_{i,j}, \dots)^\top \in \mathbb{R}^{\mathcal{N}}$, where $\vec{u}_{i,j} = [u_{i,j}^x, u_{i,j}^y]$, the problem (9) is then discretized in space, leading to a linear system

$$\partial_t c_{\varepsilon,h} = (L_h + Q_h \vec{u}_h(t/\varepsilon)) c_{\varepsilon,h}, \quad c_{\varepsilon,h}^0 = c_{\varepsilon,h}(t=0), \quad (15)$$

where L_h and Q_h are $\mathcal{N} \times \mathcal{N}$ matrices representing the discretization of the derivative and the interpolation operators. If $P_{ij} = (x_i, y_j) \in \Omega_h$ is an internal grid point (as in Fig. 3 (a)), we discretize the diffusion and advection terms as follows

$$\begin{aligned} L_h c_{\varepsilon,h} \Big|_{i,j} &= D \left(\frac{c_{i,j+1}^\varepsilon + c_{i,j-1}^\varepsilon + c_{i+1,j}^\varepsilon + c_{i-1,j}^\varepsilon - 4c_{i,j}^\varepsilon}{h^2} \right) \\ Q_h (\vec{u}_h(t/\varepsilon) c_{\varepsilon,h}) \Big|_{i,j} &= \frac{u_{i+i,j}^x c_{i+1,j}^\varepsilon - u_{i-i,j}^x c_{i-1,j}^\varepsilon + u_{i,j+1}^y c_{i,j+1}^\varepsilon - u_{i,j-1}^y c_{i,j-1}^\varepsilon}{2h} \end{aligned} \quad (16)$$

To close the linear system, we must write an equation for each ghost point. If $G = (x_i, y_j) \in \mathcal{G}_h$ is a ghost point, then we discretize the boundary condition in (11) for $\Gamma_{\mathcal{B}}$, following a ghost-point approach similar to the one proposed in [8, 10], and summarised as follows. We first compute the closest boundary point $B \in \Gamma_{\mathcal{B}}$ by

$$B = O + R_{\mathcal{B}} \frac{O - G}{|O - G|},$$

where O is the center of the bubble. Then, we identify the upwind nine-point stencil starting from $G = (x_G, y_G) = (x_i, y_j)$, containing $B = (x_B, y_B)$:

$$\{(x_{i+s_x m_x}, x_{j+s_y m_y}) : m_x, m_y = 0, 1, 2\},$$

where $s_x = \text{SGN}(x_B - x_G)$ and $s_y = \text{SGN}(y_B - y_G)$. The solution $c_{\varepsilon,h}$ and its first and second derivatives are then interpolated at the boundary point B using the discrete values $c_{i,j}^\varepsilon$ on the nine-point stencil. We start defining (see Fig. 3 (b))

$$\vartheta_x = s_x(x_B - x_G)/h, \quad \vartheta_y = s_y(y_B - y_G)/h,$$

with $0 \leq \vartheta_x, \vartheta_y < 1$. The 2D interpolation formulas are:

$$\begin{aligned}
\widehat{c}(B) &= \sum_{m_x, m_y=0}^2 l_{m_x}(\vartheta_x) l_{m_y}(\vartheta_y) c_{i+s_x m_x, j+s_y m_y}, \\
\frac{\partial \widehat{c}}{\partial x}(B) &= s_x \sum_{m_x, m_y=0}^2 l'_{m_x}(\vartheta_x) l_{m_y}(\vartheta_y) c_{i+s_x m_x, j+s_y m_y}, \\
\frac{\partial^2 \widehat{c}}{\partial x^2}(B) &= \sum_{m_x, m_y=0}^2 l''_{m_x}(\vartheta_x) l_{m_y}(\vartheta_y) c_{i+s_x m_x, j+s_y m_y}, \\
\frac{\partial^2 \widehat{c}}{\partial x \partial y}(B) &= s_x s_y \sum_{m_x, m_y=0}^2 l'_{m_x}(\vartheta_x) l'_{m_y}(\vartheta_y) c_{i+s_x m_x, j+s_y m_y}, \quad (17)
\end{aligned}$$

where

$$\begin{aligned}
l(\vartheta_\alpha) &= \left(\frac{(1-\vartheta_\alpha)(2-\vartheta_\alpha)}{2}, \vartheta_\alpha(2-\vartheta_\alpha), \frac{\vartheta_\alpha(\vartheta_\alpha-1)}{2} \right), \\
l'(\vartheta_\alpha) &= \frac{1}{h} \left(\frac{(2\vartheta_\alpha-3)}{2}, 2(1-\vartheta_\alpha), \frac{(2\vartheta_\alpha-1)}{2} \right), \quad l''(\vartheta_\alpha) = \frac{1}{h^2} (1, -2, 1), \quad \alpha = x, y,
\end{aligned}$$

and where we omit $\partial \widehat{c} / \partial y(B)$ and $\partial^2 \widehat{c} / \partial y^2(B)$ they are analogue to the x -coordinate derivatives. Finally, the rows of L_h associated with the ghost point $G = (x_G, y_G)$ are defined by evaluating the boundary condition on Γ_B , i.e.

$$L_h c_{\varepsilon, h} \Big|_B = D \Delta_\perp \widehat{c} \Big|_B - \frac{D}{\mathcal{M}} \frac{\partial \widehat{c}}{\partial n} \Big|_B, \quad (18)$$

and

$$\frac{\partial}{\partial \tau} = \tau_x \frac{\partial}{\partial x} + \tau_y \frac{\partial}{\partial y}, \quad \frac{\partial}{\partial n} = n_x \frac{\partial}{\partial x} + n_y \frac{\partial}{\partial y}, \quad (19)$$

with $(\tau_x, \tau_y) = (-n_y, n_x)$, $\cot \theta = n_x / n_y$. For a spherical bubble, $(n_x, n_y) = (O - G) / |O - G|$, $\cot \theta = x / y$.

3.2 Complex-shaped bubbles: a level-set approach

The discretization in the previous sections for the spherical bubble can be extended to more general shapes by adopting a level-set approach. In detail, the bubble \mathcal{B} can be implicitly defined by a level set function $\phi(x, y)$ that is positive inside the bubble, negative outside and zero on the boundary Γ_B (see, for example, [21, 31, 32, 33]):

$$\mathcal{B} = \{(x, y) : \phi(x, y) > 0\}, \quad \Gamma_B = \{(x, y) : \phi(x, y) = 0\}. \quad (20)$$

The unit normal vector n in (19) can be computed as $n = \frac{\nabla \phi}{|\nabla \phi|}$ where the level-set function ϕ is assumed to be explicitly known. For a spherical bubble \mathcal{B} centered at the origin, the

most convenient level-set function in terms of numerical stability is the the signed distance function between (x, y) and Γ_B , i.e. $\phi = R_B - \sqrt{x^2 + y^2}$.³

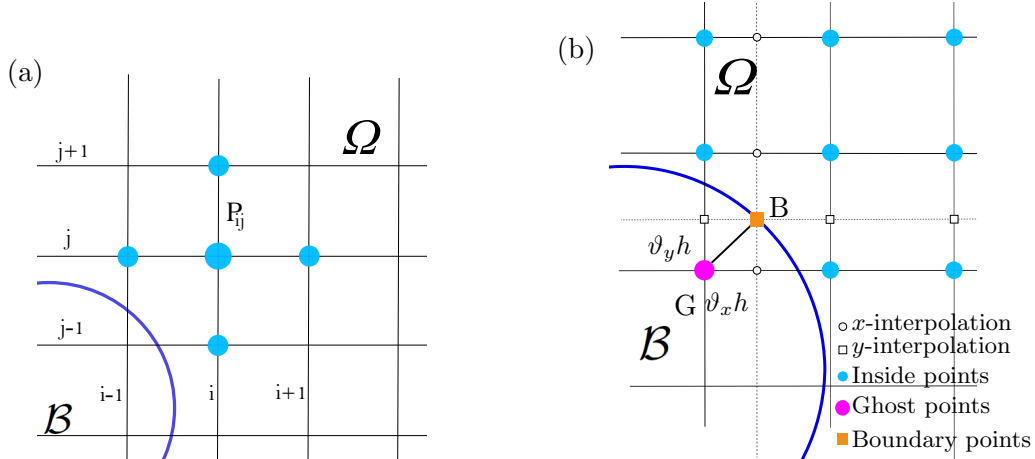


Figure 3: (a): Five-point stencil for the discrete operator L_h of the second derivatives in space for the internal points $P_{ij} = (x_i, y_j)$. (b): Representation of the Upwind nine-points stencil associated with the ghost point G , boundary point B and the relative outgoing normal vector n to Γ .

4 A two-scale formulation

In this section our goal is to provide a formal derivation of the asymptotic models for Eq. (15), to 1st and 2nd order in ε , and how the two-scale formulation can be used to derive uniformly accurate numerical schemes. The strategy is to formulate and analyze the equations obtained by decoupling the slow variable t and the fast variable $\Theta = t/\varepsilon$, following the same strategy adopted in [6, 7, 12, 13]. In this way, we obtain the two-scale formulation of Eq. (15), and then we derive the asymptotic models. Note that, one could also use the two-scale formulation to derive uniformly accurate numerical schemes solving the original equations in the vein of [6, 7, 12, 13]. Since in this paper we are solving a preliminary case, in which the velocity is explicitly known, adding a new variable Θ is not necessary. We will follow another way to construct uniformly accurate schemes.

The use of averaging methods is very common when multiple scales are involved, and the aim of the averaging is to weaken the stiffness of the short scale t/ε . We will consider a reformulation of the problem, that is more general and in which we add a degree of freedom when defining the new variable Θ . The general problem is easier to solve numerically because its initial condition can be chosen in such a way that the solution, and its first and second time derivatives, are bounded in ε .

³For arbitrary smooth level set function, and for small distances, a good approximation of the signed distance function $d(\vec{x}, t)$ is given by $d(\vec{x}, t) \approx \phi(\vec{x}, t)/|\nabla\phi(\vec{x}, t)|$.

4.1 Formal derivation of the asymptotic models: first and second order in ε

In this subsection we derive the asymptotic models for Eq. (15), to 1st and 2nd order in ε . Given $h > 0$, we consider the bounded linear operators L_h and Q_h on \mathbb{R}^N , that were defined in Section 3. Then we introduce the two-scale vector-valued function $C_h(t, \Theta) \in \mathbb{R}^N$, that is 1-periodic in Θ , and satisfies $C_h(t, t/\varepsilon) = c_{\varepsilon, h}(t)$, for all $t \geq 0$. Differentiating this quantity with respect to t , leads us to consider the following equation for $C_h(t, \Theta)$

$$\partial_t C_h(t, \Theta) + \frac{1}{\varepsilon} \partial_\Theta C_h(t, \Theta) = \mathcal{F}_\Theta(C_h(t, \Theta)), \quad C_h(0, \Theta) = C_h^0(\Theta) \quad (21)$$

where

$$\mathcal{F}_\Theta(C_h(t, \Theta)) = (L_h + Q_h \vec{u}_h(\Theta)) C_h(t, \Theta). \quad (22)$$

It is important to observe that, while the initial condition for the Eq. (15) is known, we do not have an explicit expression for $C_h^0(\Theta)$, we only know that $C_h^0(0) = c_{\varepsilon, h}^0$ where $c_{\varepsilon, h}^0$ is defined in Eq. (15). This provides us a degree of freedom in the choice of $C_h^0(\Theta)$, which is in general made in order to get a smooth solution in ε for the two-scale Eqs. (21-22). Note that, any solution to Eqs. (21-22), such that $C_h^0(0) = c_{\varepsilon, h}^0$, provides the solution of the original problem $c_{\varepsilon, h}(t) = C_h(t, t/\varepsilon)$.

Here we perform the asymptotic analysis starting from the following decomposition of $C_h(t, \Theta)$

$$C_h(t, \Theta) = \bar{C}_h(t) + \tilde{C}_h(t, \Theta), \quad (23)$$

with the choice of $\bar{C}_h(t)$ and $\tilde{C}_h(t, \Theta)$

$$\bar{C}_h(t) = \langle C(t, \bullet) \rangle \equiv \int_0^1 C_h(t, \Theta) d\Theta, \quad \langle \tilde{C}_h(t, \bullet) \rangle = 0 \quad \forall t. \quad (24)$$

Now we search for the expression of $\tilde{C}_h(t, \Theta)$. To do this, we substitute the expression (23) in Eq. (21), that becomes

$$\partial_t \bar{C}_h(t) + \partial_t \tilde{C}_h(t, \Theta) + \frac{1}{\varepsilon} \partial_\Theta \tilde{C}_h(t, \Theta) = \mathcal{F}_\Theta(\bar{C}_h(t) + \tilde{C}_h(t, \Theta)) \quad (25)$$

while the average of the Eq. (25) satisfies

$$\partial_t \bar{C}_h(t) = \langle \mathcal{F}_\bullet(\bar{C}_h(t) + \tilde{C}_h(t, \bullet)) \rangle, \quad (26)$$

with $\langle \mathcal{F}_\bullet(\bar{C}_h(t) + \tilde{C}_h(t, \bullet)) \rangle = \int_0^1 \mathcal{F}_{\Theta'}(\bar{C}_h(t) + \tilde{C}_h(t, \Theta')) d\Theta'$.

Now we subtract Eq. (26) from Eq. (25)

$$\partial_t \tilde{C}_h(t, \Theta) + \frac{1}{\varepsilon} \partial_\Theta \tilde{C}_h(t, \Theta) = \mathcal{F}_\Theta(\bar{C}_h(t) + \tilde{C}_h(t, \Theta)) - \langle \mathcal{F}_\bullet(\bar{C}_h(t) + \tilde{C}_h(t, \bullet)) \rangle,$$

and after integrating over the interval $[0, \Theta]$, we obtain

$$\tilde{C}_h(t, \Theta) = \varepsilon \int_0^\Theta \left(\mathcal{F}_\sigma(\bar{C}_h(t) + \tilde{C}_h(t, \sigma)) - \langle \mathcal{F}_\bullet(\bar{C}_h(t) + \tilde{C}_h(t, \bullet)) \rangle - \partial_t \tilde{C}_h(t, \sigma) \right) d\sigma + k(t),$$

where $k(t)$ is constant in Θ , and from Eq. (24), we deduce that

$$k(t) = -\varepsilon \left\langle \int_0^\Theta \left(\mathcal{F}_\sigma(\bar{C}_h(t) + \tilde{C}_h(t, \sigma)) - \langle \mathcal{F}_\bullet(\bar{C}_h(t) + \tilde{C}_h(t, \bullet)) \rangle - \partial_t \tilde{C}_h(t, \sigma) \right) d\sigma \right\rangle.$$

At the end, the expression for $\tilde{C}_h(t, \Theta)$ reads

$$\tilde{C}_h(t, \Theta) = \varepsilon (I - \langle \cdot \rangle) \int_0^\Theta \left(\mathcal{F}_\sigma(\bar{C}_h(t)) - \langle \mathcal{F}_\bullet(\bar{C}_h(t)) \rangle \right) d\sigma + O(\varepsilon^2), \quad (27)$$

where we used that we formally have $\tilde{C}_h(t, \Theta) = O(\varepsilon)$ and $\partial_t \tilde{C}_h(t, \Theta) = O(\varepsilon)$, uniformly in ε .

At this point, the decomposition of the solution C_h in Eq. (23) can be rewritten as an expansion in ε , as follows

$$C_h = \bar{C}_h(t) + \varepsilon C_h^1(t, \Theta) + O(\varepsilon^2) \quad (28)$$

where

$$C_h^1(t, \Theta) = (I - \langle \cdot \rangle) \int_0^\Theta \left(\mathcal{F}_\sigma(\bar{C}_h(t)) - \langle \mathcal{F}_\bullet(\bar{C}_h(t)) \rangle \right) d\sigma. \quad (29)$$

Now we want to derive an approximate equation for \bar{C}_h , to 1st and 2nd order in ε , and we obtain it by substituting $C_h^1(t, \Theta)$ in Eq. (26)

$$\partial_t \bar{C}_h(t) = \langle \mathcal{F}_\bullet(\bar{C}_h(t) + \varepsilon C_h^1(t, \bullet)) \rangle + O(\varepsilon^2). \quad (30)$$

To close the system, we need to find a good choice for the initial condition, and we derive it from Eqs. (28-29). We choose

$$C_h^0(\Theta) = \bar{C}_h(0) + \varepsilon (I - \langle \cdot \rangle) \int_0^\Theta \left(\mathcal{F}_\sigma(\bar{C}_h(0)) - \langle \mathcal{F}_\bullet(\bar{C}_h(0)) \rangle \right) d\sigma, \quad (31)$$

and if we evaluate Eq. (31) in $\Theta = 0$, with the assumption that $C_h^0(0) = c_{\varepsilon, h}^0$, we obtain

$$\begin{aligned} \bar{C}_h(0) &= c_{\varepsilon, h}^0 + \varepsilon \left\langle \int_0^\bullet \left(\mathcal{F}_\sigma(\bar{C}_h(0)) - \langle \mathcal{F}_\bullet(\bar{C}_h(0)) \rangle \right) d\sigma \right\rangle \\ &= c_{\varepsilon, h}^0 + \varepsilon \left\langle \int_0^\bullet \left(\mathcal{F}_\sigma(c_{\varepsilon, h}^0) - \langle \mathcal{F}_\bullet(c_{\varepsilon, h}^0) \rangle \right) d\sigma \right\rangle + O(\varepsilon^2). \end{aligned} \quad (32)$$

At the end, we substitute Eq. (32) in Eq. (31), obtaining the initial condition $C_h^0(\Theta)$ as a function of the initial datum $c_{\varepsilon,h}^0$ of the Eq. (15)

$$C_h^0(\Theta) = c_{\varepsilon,h}^0 + \varepsilon \int_0^\Theta (\mathcal{F}_\sigma(c_{\varepsilon,h}^0) - \langle \mathcal{F}_\bullet(c_{\varepsilon,h}^0) \rangle) d\sigma + O(\varepsilon^2). \quad (33)$$

Finally, we have all the ingredients to write the asymptotic models, to 1st and 2nd order in ε :

i) The 1st-order model reads

$$\partial_t \bar{C}_h(t) = \langle \mathcal{F}_\bullet(\bar{C}_h(t)) \rangle \quad \text{in } \Omega_h, \forall t > 0 \quad (34)$$

$$\bar{C}_h(t=0) = c_{\varepsilon,h}^0 \quad (35)$$

where $\langle \mathcal{F}_\bullet(\bar{C}_h) \rangle = \langle (L_h + Q_h \bar{u}_h(\bullet)) \bar{C}_h(t) \rangle$, and, from Eq. (28), $C_h = \bar{C}_h(t)$ is the truncation of the exact solution of Eq. (9), up to first order in ε .

ii) The 2nd-order model reads

$$\partial_t \bar{C}_h(t) = \langle \mathcal{F}_\bullet(\bar{C}_h + \varepsilon C_h^1) \rangle \quad \text{in } \Omega_h, \forall t \quad (36)$$

$$\bar{C}_h(t=0) = c_{\varepsilon,h}^0 + \varepsilon \int_0^\Theta (\mathcal{F}_\sigma(c_{\varepsilon,h}^0) - \langle \mathcal{F}_\bullet(c_{\varepsilon,h}^0) \rangle) d\sigma \quad (37)$$

where $\langle \mathcal{F}_\bullet(\bar{C}_h + \varepsilon C_h^1) \rangle = \langle (L_h + Q_h \bar{u}_h(\bullet)) (1 + \varepsilon Q_h \int_0^\bullet \bar{u}_h(\sigma) d\sigma) \bar{C}_h(t) \rangle$, and to obtain a second order approximation of the exact solution, we calculate

$$C_h(t, \Theta) = \left(1 + \varepsilon (I - \langle \cdot \rangle) \int_0^\Theta (\mathcal{F}_\sigma(\bar{C}_h(t)) - \langle \mathcal{F}_\bullet(\bar{C}_h(t)) \rangle) d\sigma \right) \bar{C}_h(t), \quad (38)$$

where, an explicit expression of the RHS is obtained by substituting the expression of \mathcal{F}_Θ in Eq. (22)

$$C_h(t, \Theta) = \left(1 + \varepsilon Q_h \int_0^\Theta \bar{u}_h(\sigma) d\sigma \right) \bar{C}_h(t). \quad (39)$$

4.2 A class of numerical schemes derived from the two-scale equation

Here we show how to derive a uniformly accurate first and second order scheme for Eq. (15) with a two-scale formulation, though in this paper we choose another strategy. Our approach is based on a suitable time integral formulation and avoids the additional variable $\Theta = t/\varepsilon$. This variable could indeed increase the complexity of the numerical schemes.

First we solve

$$\partial_t C_h(t, \Theta) + \frac{1}{\varepsilon} \partial_\Theta C_h(t, \Theta) = \mathcal{F}_\Theta(C_h(t, \Theta)) \quad \text{in } \Omega_h, \forall t > 0 \quad (40)$$

$$C_h(0, \Theta) = C_h^0(\Theta) = c_{\varepsilon,h}^0 \quad (41)$$

where the solution $C_h(t, \Theta)$ of this problem, and its first time derivative, are uniformly bounded in ε . One can construct a first order uniformly accurate scheme for Eq. (15) starting from (40-41), and then setting $c_{\varepsilon,t}(t) = C_h(t, t/\varepsilon)$ (see, for instance, [13]).

To obtain a second order scheme, we solve the following

$$\partial_t C_h(t, \Theta) + \frac{1}{\varepsilon} \partial_\Theta C_h(t, \Theta) = \mathcal{F}_\Theta(C_h(t, \Theta)) \quad \text{in } \Omega_h, \forall t > 0 \quad (42)$$

$$C_h(0, \Theta) = c_{\varepsilon,h}^0 + \varepsilon \int_0^\Theta (\mathcal{F}_\sigma(c_{\varepsilon,h}^0) - \langle \mathcal{F}_\bullet(c_{\varepsilon,h}^0) \rangle) d\sigma \quad (43)$$

where the solution $C_h(t, \Theta)$ of this problem and its time derivatives, to first and second order, are uniformly bounded with respect to ε . Therefore, one can construct a second order uniformly accurate scheme for Eq. (15) by first solving (42-43), and then setting $c_{\varepsilon,t}(t) = C_h(t, t/\varepsilon)$.

We do not apply this strategy here but we will use it in a more involved case where our model should be coupled with Stokes equations. This task is deferred to a work already under investigation.

5 First order accurate scheme, uniformly in ε

In this section we construct a scheme to solve Eq. (15), that is first order accurate in time, and we prove that it is also uniformly accurate in ε . The only property that we use is that the first time derivative of the solution is uniformly bounded in ε , and this property is justified since we assume that the initial condition is not oscillatory in space and the boundary conditions for the concentration are not oscillatory in time.

In this section we define the operator $\mathcal{A}_{\Delta t}^1$ as a sum of three sparse matrices, the identity I and the two tri-diagonal block matrices, L_h and Q_h , defined in Eqs. (16). In this way, it is easy to solve the linear system in Eq. (45) with standard numerical techniques.

Proposition 1. *Let L_h and Q_h be bounded operators in \mathbb{R}^N defined in Section 3, with $h > 0$. Let $c_{\varepsilon,h}^0 \in \mathbb{R}^N$ be bounded in ε , $\vec{u}_h \in \mathbb{R}^N$ be a bounded given 1-periodic function of time. Then, there exists a constant $\Delta t_0 > 0$ independent of ε such that, for all $\Delta t < \Delta t_0$, the following holds true:*

i) *The operator $\mathcal{A}_{\Delta t}^1 := I - \Delta t L_h - Q_h \int_{t^n}^{t^{n+1}} \vec{u}_h(s/\varepsilon) ds$ in \mathbb{R}^N is invertible.*

ii) *The following:*

$$c_{\varepsilon,h}^0 = c_{\varepsilon,h}(0), \quad (44)$$

$$c_{\varepsilon,h}^{n+1} = \mathcal{A}_{\Delta t}^1{}^{-1} c_{\varepsilon,h}^n, \quad (45)$$

for $n = 1, \dots, M$ is a first order scheme, uniformly accurate with respect to ε , solving the Eq. (15). In other words, we have $\|c(t^n) - c^n\| \leq K \Delta t$ for all $n = 1, \dots, M$, with K independent of ε , $\Delta t = t_{\text{fin}}/M$, $t_{\text{fin}} > 0$ and $t^n = n \Delta t$.

Proof. To prove i), we first show that $\mathcal{A}_{\Delta t}^1 \rightarrow I$, when $\Delta t \rightarrow 0$ since the operators L_h and Q_h , and the function \vec{u}_h are bounded. Thus there exists a constant $\widehat{K} > 0$ (independent of ε), such that, $\forall \Delta t < \widehat{K}$, $\det(\mathcal{A}_{\Delta t}^1) \neq 0$, and $\mathcal{A}_{\Delta t}^1$ is invertible.

To prove ii), we first show how to deduce the scheme defined in Eqs. (44-45). We start integrating Eq. (15) between t and t^{n+1} , with $[t, t^{n+1}] \subset [t^n, t_{\text{fin}}]$

$$c_{\varepsilon,h}(t^{n+1}) - c_{\varepsilon,h}(t) = \int_t^{t^{n+1}} (L_h + Q_h \vec{u}_h(s/\varepsilon)) c_{\varepsilon,h}(s) ds. \quad (46)$$

Evaluating the quantity $c_{\varepsilon,h}(t)$ in $t = t^n$, we obtain

$$c_{\varepsilon,h}(t^{n+1}) - c_{\varepsilon,h}(t^n) = \int_{t^n}^{t^{n+1}} (L_h + Q_h \vec{u}_h(s/\varepsilon)) c_{\varepsilon,h}(s) ds, \quad (47)$$

and then the following

$$c_{\varepsilon,h}(t^{n+1}) - c_{\varepsilon,h}(t^n) \approx \left(\int_{t^n}^{t^{n+1}} (L_h + Q_h \vec{u}_h(s/\varepsilon)) ds \right) c_{\varepsilon,h}(t^{n+1}). \quad (48)$$

Since the operators L_h and Q_h do not depend on time, Eq. (48) becomes

$$c_{\varepsilon,h}(t^{n+1}) - c_{\varepsilon,h}(t^n) \approx L_h \Delta t c_{\varepsilon,h}(t^{n+1}) + Q_h c_{\varepsilon,h}(t^{n+1}) \int_{t^n}^{t^{n+1}} \vec{u}_h(s/\varepsilon) ds \quad (49)$$

where the integral $\int_{t^n}^{t^{n+1}} \vec{u}_h(s/\varepsilon) ds$ is calculated analytically. At the end, the scheme reads

$$c_{\varepsilon,h}^{n+1} - c_{\varepsilon,h}^n = L_h \Delta t c_{\varepsilon,h}^{n+1} + Q_h c_{\varepsilon,h}^{n+1} \int_{t^n}^{t^{n+1}} \vec{u}_h(s/\varepsilon) ds \quad (50)$$

where $c_{\varepsilon,h}^n \approx c_{\varepsilon,h}(t^n)$.

Now we prove that the scheme in Eq. (50) is first order in Δt , uniformly in ε . We subtract Eq. (50) from Eq. (47), define the error at time t^n as $e_n = c_{\varepsilon,h}(t^n) - c_{\varepsilon,h}^n$, and obtain

$$e_{n+1} - e_n = \int_{t^n}^{t^{n+1}} (L_h + Q_h \vec{u}_h(s/\varepsilon)) (c_{\varepsilon,h}(s) - c_{\varepsilon,h}^{n+1}) ds. \quad (51)$$

Here we substitute $c_{\varepsilon,h}(s) - c_{\varepsilon,h}^{n+1} = c_{\varepsilon,h}(s) - c_{\varepsilon,h}(t^{n+1}) + c_{\varepsilon,h}(t^{n+1}) - c_{\varepsilon,h}^{n+1}$ in Eq. (51), obtaining

$$\begin{aligned} e_{n+1} - e_n &= \int_{t^n}^{t^{n+1}} (L_h + Q_h \vec{u}_h(s/\varepsilon)) (c_{\varepsilon,h}(s) - c_{\varepsilon,h}(t^{n+1})) ds \\ &\quad + \int_{t^n}^{t^{n+1}} (L_h + Q_h \vec{u}_h(s/\varepsilon)) ds (c_{\varepsilon,h}(t^{n+1}) - c_{\varepsilon,h}^{n+1}). \end{aligned} \quad (52)$$

Since $\vec{u}_h(t/\varepsilon)$ and $c_{\varepsilon,h}(t)$ are bounded, also the first derivative in time of $c_{\varepsilon,h}(t)$ is bounded, i.e., there exists a constant K_1 , independent of ε , such that

$$\|\partial_t c_{\varepsilon,h}\|_{\mathcal{L}^\infty(\Omega)} = \|(L_h + Q_h \vec{u}_h(t/\varepsilon)) c_{\varepsilon,h}\|_{\mathcal{L}^\infty(\Omega)} < K_1.$$

where $K_1 = (\|L_h\| + \|Q_h\| \|u\|_\infty) \|c_{\varepsilon,h}\|_{\mathcal{L}^\infty(\Omega)}$. From this estimate, we obtain

$$\|c_{\varepsilon,h}(s) - c_{\varepsilon,h}(t^{n+1})\| \leq K_1 \|s - t^{n+1}\| \leq K_1 \Delta t, \quad \forall s \in [t^n, t^{n+1}]. \quad (53)$$

Now we consider the first term of the RHS of Eq. (52), that is bounded by

$$\left\| \int_{t^n}^{t^{n+1}} (L_h + Q_h \vec{u}_h(s/\varepsilon)) (c_{\varepsilon,h}(s) - c_{\varepsilon,h}(t^{n+1})) ds \right\| \leq K_1 K_2 \Delta t^2 \quad (54)$$

where $K_2 = \|L_h + Q_h \vec{u}_h(s/\varepsilon)\|_{\mathcal{L}^\infty(\Omega)}$, and, it does not depend on ε .

Considering now the norm of the Eq. (52), the following inequalities hold

$$\|e_{n+1}\| - \|e_n\| \leq \|e_{n+1} - e_n\| \leq K_1 K_2 \Delta t^2 + \|e_{n+1}\| K_2 \Delta t \leq K_3 \Delta t^2 + \|e_{n+1}\| K_3 \Delta t, \quad (55)$$

where $K_3 = \max\{K_1 K_2, K_2\}$. After some algebra, adding Δt in both sides, and defining $E_n = \|e_n\|$, we have

$$E_{n+1} + \Delta t \leq (1 - K_3 \Delta t)^{-1} (E_n + \Delta t). \quad (56)$$

if, and only if, $\Delta t < 1/K_3$. From Eq. (56), recursively to $E_0 = 0$, we obtain that

$$E_n + \Delta t \leq (1 - K_3 \Delta t)^{-n} \Delta t \leq \left(1 - K_3 \frac{t_{\text{fin}}}{N}\right)^{-N} \Delta t$$

which follows that, there exists a constant K_4 , such that

$$E_n \leq \left(\left(1 - K_3 \frac{t_{\text{fin}}}{N}\right)^{-N} - 1 \right) \Delta t \leq K_4 \Delta t$$

K_4 independent of N , since $\lim_{N \rightarrow +\infty} \left((1 - K_3 t_{\text{fin}}/N)^{-N} - 1 \right) = \exp(K_3 t_{\text{fin}}) - 1$.

To conclude the proof, we define $\Delta t_0 = \min\{\widehat{K}, 1/K_3\}$. □

6 Second order accurate scheme, uniformly in ε

In this section we construct a scheme to solve Eq. (15), that is second order accurate in time, and we prove that is also uniformly accurate in ε . To do this, we follow the approach showed in Section 5 and the only property that we use is that the first time derivative of the solution is uniformly bounded in ε , justified from the assumption that the initial condition is not oscillatory in space and the boundary conditions are not oscillatory in time. We also show how to deal with the integration of the Laplacian operator in the proof of Proposition 2. In Remark 2 we also show other alternatives.

Proposition 2. Let L_h and Q_h be finite dimensional bounded operators in \mathbb{R}^N defined in Section 3, with $h > 0$. Let $c_{\varepsilon,h}^0 \in \mathbb{R}^N$ be bounded in ε , and let $\vec{u}_h \in \mathbb{R}^N$ be a bounded given 1-periodic function in time. Then, there exists a constant $\Delta t_0 > 0$ independent of ε , such that for all $\Delta t < \Delta t_0$, the following holds true:

i) The operator $\mathcal{A}_{\Delta t}^2 = I - \mathbb{M}$ in \mathbb{R}^N is invertible, where

$$\begin{aligned} \mathbb{M} &= L_h \Delta t + Q_h \int_{t^n}^{t^{n+1}} \vec{u}_h(s/\varepsilon) ds - \frac{1}{2} L_h^2 \Delta t^2 \\ &\quad - L_h Q_h \int_{t^n}^{t^{n+1}} \int_s^{t^{n+1}} \vec{u}_h(\sigma/\varepsilon) d\sigma ds - Q_h L_h \int_{t^n}^{t^{n+1}} (t^{n+1} - s) \vec{u}_h(s/\varepsilon) ds \\ &\quad - Q_h^2 \int_{t^n}^{t^{n+1}} \vec{u}_h(s/\varepsilon) \int_s^{t^{n+1}} \vec{u}_h(\sigma/\varepsilon) d\sigma ds, \end{aligned}$$

ii) The following scheme:

$$c_{\varepsilon,h}^0 = c_{\varepsilon,h}(0), \quad (57)$$

$$c_{\varepsilon,h}^{n+1} = \mathcal{A}_{\Delta t}^2{}^{-1} c_{\varepsilon,h}^n, \quad \text{for } n = 1, \dots, M \quad (58)$$

is a second order scheme, uniformly accurate with respect to ε , solving the Eq. (15). In other words we have $\|c(t^n) - c^n\| \leq K \Delta t^2$, for all $n = 1, \dots, M$, with K independent of ε , $t^n = n \Delta t$ and $\Delta t = t_{\text{fin}}/M$.

Proof. To prove i), we prove that $\mathcal{A}_{\Delta t}^2$ is invertible when $\Delta t \rightarrow 0$. We start considering the norm of the operator $\mathcal{A}_{\Delta t}^2$ as before, and, analogously, since the operators L_h and Q_h are bounded in \mathbb{R}^N , and the vector-valued function \vec{u}_h is also bounded, it follows that $\|\mathcal{A}_{\Delta t}^2\| \rightarrow \|I\|$ when $\Delta t \rightarrow 0$. Thus, following the same procedure as before, we say that there exists a constant $\widehat{K} > 0$, such that, $\forall \Delta t < \widehat{K}$, the operator $\mathcal{A}_{\Delta t}^2$ is invertible.

To prove ii), we first show how to deduce the scheme defined in Eqs. (57-58). First, we substitute $c_{\varepsilon,h}(t)$ with $c_{\varepsilon,h}(s)$ in Eq. (46), and it can be rewritten as

$$c_{\varepsilon,h}(s) = c_{\varepsilon,h}(t^{n+1}) - \int_s^{t^{n+1}} (L_h + Q_h \vec{u}_h(\sigma/\varepsilon)) c_{\varepsilon,h}(\sigma) d\sigma, \quad (59)$$

where we remind that the choice of integrating between t and t^{n+1} , with $t < t^{n+1}$, is our strategy to obtain a negative sign in front of the operator L_h^2 in Eq. (62) (see Remark 2 for more details).

Now we substitute Eq. (59) in Eq. (46), as follows

$$\begin{aligned} c_{\varepsilon,h}(t^{n+1}) - c_{\varepsilon,h}(t) &= \int_t^{t^{n+1}} (L_h + Q_h \vec{u}_h(s/\varepsilon)) c_{\varepsilon,h}(s) ds \\ &= \int_t^{t^{n+1}} (L_h + Q_h \vec{u}_h(s/\varepsilon)) \left(c_{\varepsilon,h}(t^{n+1}) - \int_s^{t^{n+1}} (L_h + Q_h \vec{u}_h(\sigma/\varepsilon)) c_{\varepsilon,h}(\sigma) d\sigma \right) ds, \end{aligned}$$

we evaluate the quantity $c_{\varepsilon,h}(t)$ in $t = t^n$

$$c_{\varepsilon,h}(t^{n+1}) - c_{\varepsilon,h}(t^n) = \int_{t^n}^{t^{n+1}} (L_h + Q_h \vec{u}_h(s/\varepsilon)) \left(c_{\varepsilon,h}(t^{n+1}) - \int_s^{t^{n+1}} (L_h + Q_h \vec{u}_h(\sigma/\varepsilon)) c_{\varepsilon,h}(\sigma) d\sigma \right) ds \quad (60)$$

and we approximate the equation in the following way

$$c_{\varepsilon,h}^{n+1} - c_{\varepsilon,h}^n = \int_{t^n}^{t^{n+1}} (L_h + Q_h \vec{u}_h(s/\varepsilon)) \left(c_{\varepsilon,h}^{n+1} - \int_s^{t^{n+1}} (L_h + Q_h \vec{u}_h(\sigma/\varepsilon)) d\sigma c_{\varepsilon,h}^{n+1} \right) ds, \quad (61)$$

where $c_{\varepsilon,h}^n \approx c_{\varepsilon,h}(t^n)$. Going on with the computations of the integrals, we have

$$\begin{aligned} c_{\varepsilon,h}^{n+1} - c_{\varepsilon,h}^n &= \Delta t L_h c_{\varepsilon,h}^{n+1} + Q_h c_{\varepsilon,h}^{n+1} \int_{t^n}^{t^{n+1}} \vec{u}_h(s/\varepsilon) ds - \frac{1}{2} \Delta t^2 L_h^2 c_{\varepsilon,h}^{n+1} \\ &- L_h Q_h c_{\varepsilon,h}^{n+1} \int_{t^n}^{t^{n+1}} \int_s^{t^{n+1}} \vec{u}_h(\sigma/\varepsilon) d\sigma ds - Q_h L_h c_{\varepsilon,h}^{n+1} \int_{t^n}^{t^{n+1}} (t^{n+1} - s) \vec{u}_h(s/\varepsilon) ds \\ &- Q_h^2 c_{\varepsilon,h}^{n+1} \int_{t^n}^{t^{n+1}} \vec{u}_h(s/\varepsilon) \int_s^{t^{n+1}} \vec{u}_h(\sigma/\varepsilon) d\sigma ds. \end{aligned} \quad (62)$$

At this point, we show that the numerical scheme is second order accurate, uniformly in ε . Here we subtract Eq. (61) from Eq. (60), as before, obtaining

$$\begin{aligned} e_{n+1} - e_n &= \int_{t^n}^{t^{n+1}} (L_h + Q_h \vec{u}_h(s/\varepsilon)) e_{n+1} ds \\ &- \int_{t^n}^{t^{n+1}} (L_h + Q_h \vec{u}_h(s/\varepsilon)) \int_s^{t^{n+1}} (L_h + Q_h \vec{u}_h(\sigma/\varepsilon)) (c_{\varepsilon,h}(\sigma) - c_{\varepsilon,h}^{n+1}) d\sigma ds. \end{aligned} \quad (63)$$

where, again, $e_n = c_{\varepsilon,h}(t^n) - c_{\varepsilon,h}^n$. Now we add and subtract the same quantity to the RHS as before, $c_{\varepsilon,h}(s) - c_{\varepsilon,h}^{n+1} = c_{\varepsilon,h}(s) - c_{\varepsilon,h}(t^{n+1}) + c_{\varepsilon,h}(t^{n+1}) - c_{\varepsilon,h}^{n+1}$ and, using the analogue procedure and the same constants seen in Eq. (55), Eq. (63) becomes

$$(1 - K_3 \Delta t - K_3^2 \Delta t^2) E_{n+1} - K_3 \Delta t^3 \leq E_n$$

where $E_n = \|e_n\|$.

In this case, we add $\Delta t^2/(K_3 \Delta t + 1)$ to both sides, and, after some algebra, the inequality reads

$$E_{n+1} + \frac{\Delta t^2}{K_3 \Delta t + 1} \leq (1 - K_3 \Delta t - K_3^2 \Delta t^2)^{-1} \left(E_n + \frac{\Delta t^2}{K_3 \Delta t + 1} \right),$$

if $K_3\Delta t(1 + K_3\Delta t) < 1$. Recursively we obtain (using $E_0 = 0$)

$$E_n + \frac{\Delta t^2}{K\Delta t + 1} \leq (1 - K_3\Delta t - K_3^2\Delta t^2)^{-n} \frac{\Delta t^2}{K_3\Delta t + 1}.$$

As before, it is easy to show that there exists a constant \widehat{K} that does not depend on N , such that $E_n \leq \widehat{K}\Delta t^2$. To conclude the proof, we define $\Delta t_0 = \min\{\widehat{K}, \widetilde{K}\}$, where \widetilde{K} is the positive solution of the equation $1 - K_3\Delta t - K_3^2\Delta t^2 = 0$. \square

Remark 2. We noticed that, the choice of the time interval for the integration of Eq. (15) can be trivial, because the wrong integration can bring instability to the numerical scheme. We need a negative sign in front of the term $(L_h \Delta t)^2 / 2$ in Eq. (62), since the operator L_h represents the discrete Laplacian in space. Here we show some examples in which some instability can be generated.

Let us consider the integration of Eq. (15) between t^n and t , and between t and t^{n+1} , with $t^n < t < t^{n+1}$

$$c_{\varepsilon,h}(t) = c_{\varepsilon,h}(t^n) + \int_{t^n}^t (L_h + Q_h \vec{u}_h(s/\varepsilon)) c_{\varepsilon,h}(s) ds \quad (64)$$

$$c_{\varepsilon,h}(t) = c_{\varepsilon,h}(t^{n+1}) - \int_t^{t^{n+1}} (L_h + Q_h \vec{u}_h(s/\varepsilon)) c_{\varepsilon,h}(s) ds. \quad (65)$$

The first possibility is that we iterate Eq. (64) in itself, but in this case it is obvious that a negative sign will not appear. The second possibility is to substitute $c_{\varepsilon,h}(s)$ in Eq. (65) with $c_{\varepsilon,h}(t)$ in Eq. (64) to expand the integrand, obtaining

$$c_{\varepsilon,h}(t^{n+1}) = c_{\varepsilon,h}(t^n) + \int_{t^n}^{t^{n+1}} (L_h + Q_h \vec{u}_h(s/\varepsilon)) \left(c_{\varepsilon,h}(t^n) + \int_{t^n}^s (L_h + Q_h \vec{u}_h(\sigma/\varepsilon)) c_{\varepsilon,h}(\sigma) d\sigma \right) ds, \quad (66)$$

in which, again, we do not obtain a negative sign.

The third possibility is to report Eq. (65) in Eq. (65), and it is the one that we show in Proposition 2.

7 Numerical results

In this section we confirm the numerical orders of convergence, uniformly in ε , of the integral-type schemes in Eqs. (44-45) and (57-58). We also show different tests, changing the expression for the velocity $\vec{u}_{\varepsilon,h}$, and we confirm our previous assumptions about the space oscillations, in Remark 1.

The domain considered in the following tests is $\Omega = ([-1, 1] \times [-1, 1]) \setminus \mathcal{B}$, where \mathcal{B} is a circle centered in $(0, 0)$ with radius $R_{\mathcal{B}} = 0.2$. The expression for the initial condition used in the computations is the following

$$c_{\varepsilon,h}^0 = c_{\varepsilon,h}(t = 0, x_h, y_h) = \exp\left(-\left(x_h^2 + (y_h - y_0)^2\right) / 2\sigma^2\right), \quad y_0, \sigma \in \mathbb{R}. \quad (67)$$

In our tests we choose the following expressions for the velocity $\vec{u}_h(t/\varepsilon)$

$$\text{TESTCOS} : \quad \vec{u}_h = AR_{\mathcal{B}} \cos(2\pi t/\varepsilon) \cdot (x_h, y_h)^\top / (x_h^2 + y_h^2) \quad (68)$$

where A is the amplitude. To show the oscillations in space, we define a test function that depends on x_h/ε

$$\text{TESTOSC} : \quad \vec{u}_h = AR_{\mathcal{B}} \cos(2\pi(t + x_h)/\varepsilon) \cdot (1, 0)^\top. \quad (69)$$

To calculate the error, we first compute a reference solution $c_{\varepsilon,h}^{\text{ref}}$, choosing related reference time step Δt_{ref} , number of points N_{ref} and final time t_{fin} , for the following set of $\varepsilon = 10^{-k}$, $k \in \{0, 1, 2, 3, 4, 5, 6\}$. Then, we calculate different solutions $c_{\varepsilon,h}^{\Delta t, N}$, for different $\Delta t = 0.01 \cdot 2^{-k}$, $k \in \{0, 1, 2, 3, 4, 5, 6\}$ and $N = 20, 40, 80, 160$. After computing all the solutions, we calculate the L^2 -norm of the relative error as follow:

$$\text{error} = \frac{\|c_{\varepsilon,h}^{\text{ref}} - c_{\varepsilon,h}^{\Delta t, N}\|_2}{\|c_{\varepsilon,h}^{\text{ref}}\|_2}. \quad (70)$$

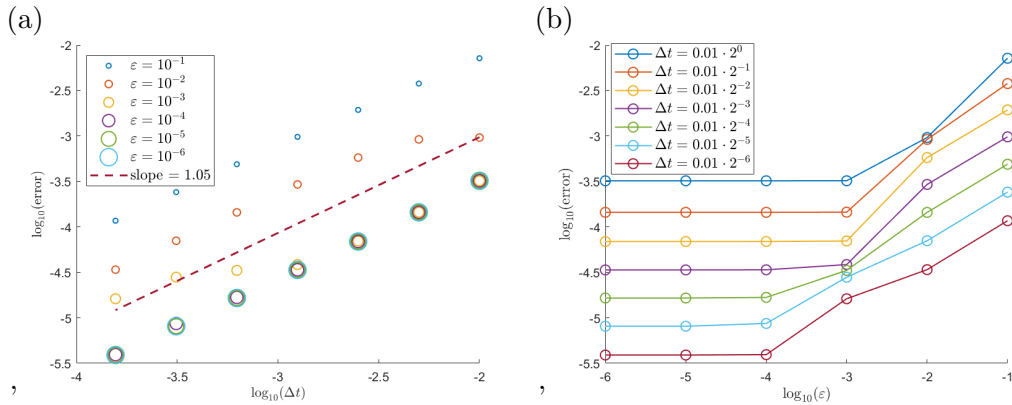


Figure 4: Plot of the relative L^2 error for the first order scheme in Eq. (50) as a function of Δt and different ε (a) and as a function of ε and different Δt (b). The parameters of the tests are: $t_{\text{fin}} = 0.1$, $\Delta t_{\text{ref}} = 10^{-5}$, $N_{\text{ref}} = 160$, $D = 0.02$, $x_0 = 1.2$, $y_0 = 0$, $\sigma = 0.2$, $\delta = 10^{-2}$, $A = 1$. The initial condition is defined in Eq. (67) and the velocity in TESTCOS.

In Fig. 4 (a) we show the L^2 -norm of the error, as a function of Δt and for different values of ε . The method that we consider here is the first order accurate numerical scheme defined

in Eq. (50). In Fig. 4 (b) we have the L^2 -norm of the error as a function of ε , for different values of Δt , to show that the numerical scheme is uniformly accurate in ε . Analogously, in Fig. 5 (a) and (b) we show that the numerical scheme defined in Eq. (62) is second order accurate, uniformly in ε .

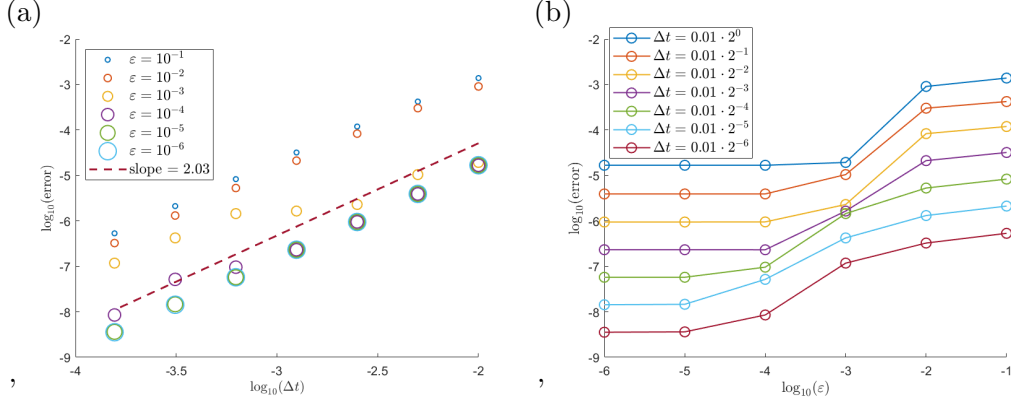


Figure 5: Plot of the relative L^2 error for the second order scheme in Eq. (62) as a function of Δt and different ε (a) and as a function of ε and different Δt (b). The parameters of the tests are: $t_{\text{fin}} = 0.1, \Delta t_{\text{ref}} = 10^{-5}, N_{\text{ref}} = 160, D = 0.02, y_0 = -1, \sigma = 0.2, \delta = 10^{-2}, A = 1$. The initial condition is defined in Eq. (67) and the velocity in TESTCOS.

In Fig. 6 we show the L^2 -norm of the error of the space discretization defined in Eq. (15). In (a) we show the error as a function of Δx for different ε , and in (b) there is the error as a function of ε , for different Δx . As expected, the numerical scheme is second order accurate, uniformly in ε .

Fig. 7 represents the time evolution of the solution at the detector using the second order scheme in Eq. (62), for the TESTCOS. We choose two different values of ε : in panel (a) $\varepsilon = 0.01$ and in panel (b) $\varepsilon = 0.001$. We show a reference solution, $c_{\varepsilon,h}^{\text{ref}}$ (blue line) with $\Delta t_{\text{ref}} = 10^{-4}$, together with different solutions for different time steps. The main goal is to show that for $\Delta t > \varepsilon$, the two concentrations, $c_{\varepsilon,h}^{\text{ref}}$ and $c_{\varepsilon,h}^{\Delta t,N}$, overlap.

In Fig. 8–9 (a), we show the comparison between the second order numerical scheme in Eq. (62) (yellow stars and red diamonds), and a direct simulation using a traditional Crank-Nicolson (CN) method (green circles), together with a reference solution (blue line). The reference solutions have been computed with a time step $\Delta t_{\text{ref}} = 2 \times 10^{-5}$, which is much smaller than the period ε . The other solutions are obtained using a time step of length which is not commensurable with the period, but is of the same order of magnitude of ε . In the zoom-in panels (b) and (c) we see the advantages of the scheme described in this paper (green stars, red diamonds). The advantage of the numerical scheme described in this paper is more evident for small values of ε , as we show in Fig. 9, with $\varepsilon = 10^{-2}$: for $\varepsilon = 10^{-1}$ accurate solutions are obtained with a time step greater than 3ε , while in the case $\varepsilon = 10^{-2}$, the method provides an accurate solution even when the time step is one order

of magnitude larger than the period (red diamonds).

As mentioned in the Remark 1, when there is a dependence on \vec{x}/ε , spatial oscillations occur, rendering the Propositions presented in this paper not valid. In Fig. 10 we show the results of the TESTOSC, considering time steps larger than ε (green circles) together with a reference solution (i.e., $N_{\text{ref}} = 200, \Delta t_{\text{ref}} = 10^{-3}$) to confirm that the accuracy is not guaranteed when we use the time integrator in (62).

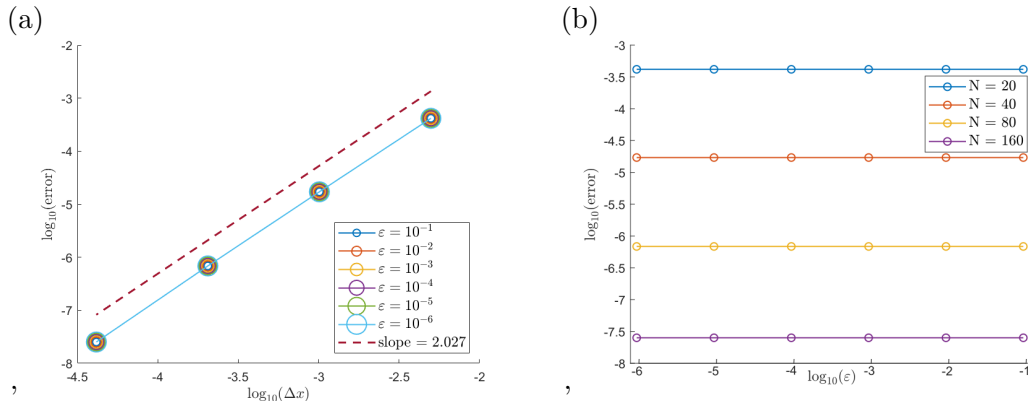


Figure 6: Plot of the relative L^2 error in space for the second order scheme in Eq. (15) as a function of Δx and different ε (a) and as a function of ε and different Δx (b). The parameters of the tests are: $t_{\text{fin}} = 0.1, \Delta t_{\text{ref}} = 10 \cdot 2^6, N_{\text{ref}} = 640, D = 0.02, y_0 = -1, \sigma = 0.2, \delta = 10^{-2}, A = 1$. The initial condition is defined in Eq. (67) and the velocity in TESTCOS.

8 Conclusions

In this work, we have presented a general strategy for constructing uniformly accurate numerical schemes for highly oscillatory advection diffusion equations, motivated by the necessity of solving the multiscale problem developed in [2] to treat the diffusion and trapping of a surfactant around a rapidly oscillatory bubble (see also [24], [9], [1]).

Traditional numerical time integrators, that are commonly employed, require significant time restrictions to achieve accurate solutions when the oscillation period is much smaller than the diffusion time, since the time step has to be smaller than the oscillation period.

Here we demonstrate that there are alternative choices available to achieve the desired accuracy without resolving the short oscillation period, thus making the computational cost orders of magnitude smaller than the one required by methods from the literature.

The accuracy of the proposed method actually improves when the oscillation frequency increases, providing accurate solutions with time steps much larger than the oscillation period.

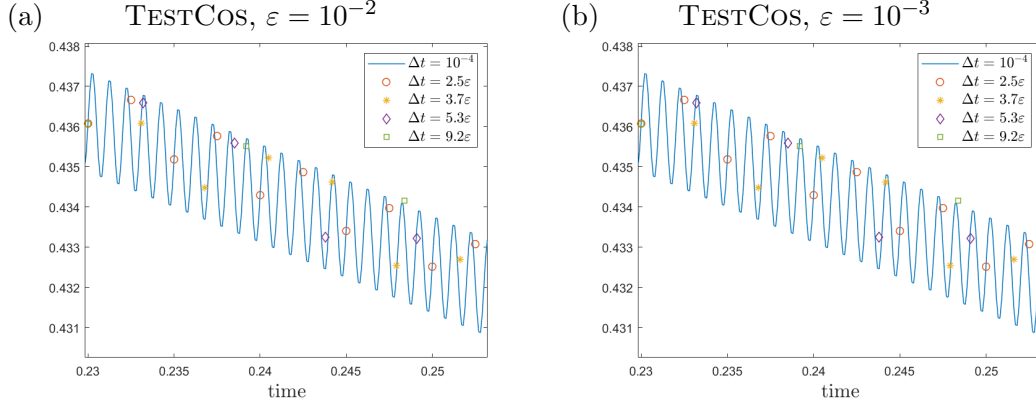


Figure 7: Concentration $c_{\epsilon,h}$ at the detector for different values of Δt with $\epsilon = 0.01$ (a) and $\epsilon = 0.001$ in (b), for TESTCOS. The initial condition is defined in Eq. (67) and the detector is centered in $P = (0, -0.5)$, $P \in \Omega$. The parameters of the test are: $N = 160$, $A = 10$, $\delta = 10^{-3}$, $y_0 = -0.75$ and $D = 0.02$.

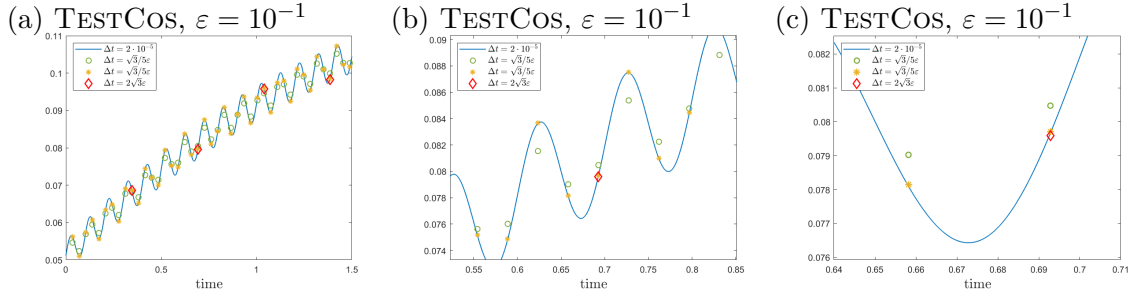


Figure 8: (a): Comparison of two different, second order accurate in time integrators for Eq. (15) for TESTCOS, together with a reference solution (blue line): integral-type scheme in Eq. (62) (yellow stars and red diamonds) and Crank-Nicolson scheme (CN) (green circles). (b): Zoom-in of panel (a). (c): Zoom-in of panel (b). The parameters of the system are: $\epsilon = 10^{-1}$, $N = 160$, $A = 1$, $D = 0.02$, $\delta = 10^{-1}$, $y_0 = -0.75$.

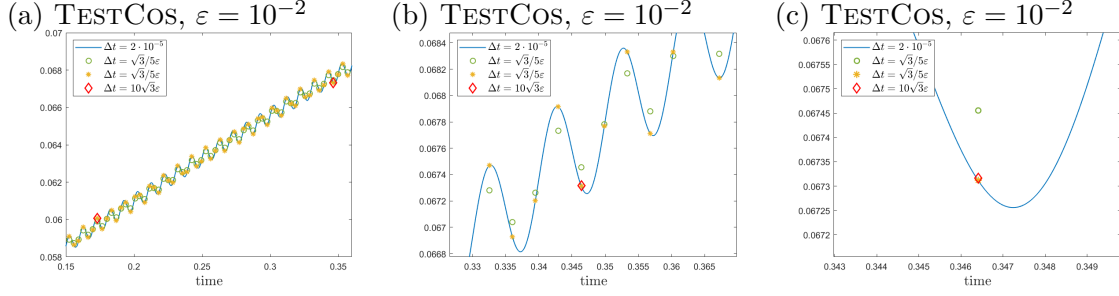


Figure 9: (a): Comparison of two different, second order accurate in time integrators for Eq. (15) for TESTCOS, together with a reference solution (blue line): integral-type scheme in Eq. (62) (yellow stars and red diamonds) and Crank-Nicolson scheme (CN) (green circles). (b): Zoom-in of panel (a). (c): Zoom-in of panel (b). The parameters of the system are: $\varepsilon = 10^{-2}$, $N = 160$, $A = 1$, $D = 0.02$, $\delta = 10^{-2}$, $y_0 = -0.75$.

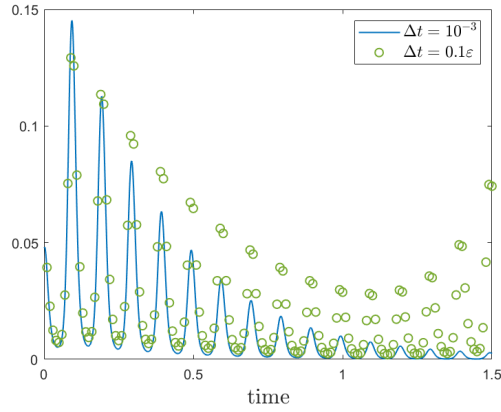


Figure 10: Detector values of the concentration $c_{\varepsilon,h}$ for TESTOSC, and different time steps Δt . The initial condition is defined in Eq. (67) and the detector is centered at $P = (0, -0.5)$, $P \in \Omega$. Parameters of the numerical test: $N = 200$, $\varepsilon = 0.1$, $A = 1$, $y_0 = -1$, $\Delta t = 10^{-3}$, $D = 0.1$ and $\delta = 10^{-3}$.

Here we assume that the fluid velocity is a known function of space and time. A natural extension of the current work is the numerical solution of a coupled Stokes-advection-diffusion system, where the expression for the velocity in the advection term is obtained numerically by solving the Stokes equations.

References

- [1] Clarissa Astuto, Armando Coco, Giovanni Russo, *A finite-difference ghost-point multigrid method for multi-scale modelling of sorption kinetics of a surfactant past an oscillating bubble*, *Journal of Computational Physics*, **476**, 111880 (2023), ISSN: 0021-9991, DOI: <https://doi.org/10.1016/j.jcp.2022.111880>, URL: <https://www.sciencedirect.com/science/article/pii/S0021999122009433>.
- [2] Clarissa Astuto, Antonio Raudino, Giovanni Russo, *Multiscale modeling of sorption kinetics*, *Multiscale Modeling & Simulation*, **21**(1), 374–399 (2023), Publisher: SIAM, DOI: <https://doi.org/10.1137/19M1269372>.
- [3] O. Bénichou, C. Loverdo, M. Moreau, R. Voituriez, *Intermittent search strategies*, *Rev. Mod. Phys.*, **83**(1), 81–129 (2011), Publisher: American Physical Society, DOI: 10.1103/RevModPhys.83.81, URL: <https://link.aps.org/doi/10.1103/RevModPhys.83.81>.
- [4] F.W Wiegel, *Diffusion and the physics of chemoreception*, *Physics Reports*, **95**(5), 283–319 (1983), DOI: [https://doi.org/10.1016/0370-1573\(83\)90078-9](https://doi.org/10.1016/0370-1573(83)90078-9).
- [5] Philippe Chartier, Nicolas Crouseilles, Mohammed Lemou, Florian Méhats, *Uniformly accurate numerical schemes for highly oscillatory Klein–Gordon and nonlinear Schrödinger equations*, *Numerische Mathematik*, **129**, 211–250 (2015), Publisher: Springer.
- [6] Philippe Chartier, Mohammed Lemou, Florian Méhats, Gilles Vilmart, *A new class of uniformly accurate numerical schemes for highly oscillatory evolution equations*, *Foundations of Computational Mathematics*, **20**, 1–33 (2020), Publisher: Springer.
- [7] Philippe Chartier, Mohammed Lemou, Florian Méhats, Xiaofei Zhao, *Derivative-free high-order uniformly accurate schemes for highly oscillatory systems*, *IMA Journal of Numerical Analysis*, **42**(2), 1623–1644 (2022), Publisher: Oxford University Press.
- [8] Armando Coco, Giovanni Russo, *Finite-difference ghost-point multigrid methods on Cartesian grids for elliptic problems in arbitrary domains*, *Journal of Computational Physics*, **241**, 464–501 (2013), ISSN: 0021-9991, DOI: <https://doi.org/10.1016/j.jcp.2012.11.047>, URL: <http://www.sciencedirect.com/science/article/pii/S0021999112007292>.

- [9] Armando Coco, *A multigrid ghost-point level-set method for incompressible Navier-Stokes equations on moving domains with curved boundaries*, *Journal of Computational Physics*, **418**, 109623 (2020), ISSN: 0021-9991, DOI: <https://doi.org/10.1016/j.jcp.2020.109623>, URL: <https://www.sciencedirect.com/science/article/pii/S0021999120303971>.
- [10] Armando Coco, Giovanni Russo, *Second order finite-difference ghost-point multigrid methods for elliptic problems with discontinuous coefficients on an arbitrary interface*, *Journal of Computational Physics*, **361**, 299–330 (2018), ISSN: 0021-9991, DOI: <https://doi.org/10.1016/j.jcp.2018.01.016>, URL: <http://www.sciencedirect.com/science/article/pii/S0021999118300263>.
- [11] M. Corti, M. Pannuzzo, A. Raudino, *Out of Equilibrium Divergence of Dissipation in an Oscillating Bubble Coated by Surfactants*, *Langmuir*, **2014**, DOI: 10.1021/1a4040062.
- [12] Nicolas Crouseilles, Mohammed Lemou, Florian Méhats, *Asymptotic preserving schemes for highly oscillatory Vlasov–Poisson equations*, *Journal of Computational Physics*, **248**, 287–308 (2013), Publisher: Elsevier.
- [13] Nicolas Crouseilles, Mohammed Lemou, Florian Méhats, Xiaofei Zhao, *Uniformly accurate forward semi-Lagrangian methods for highly oscillatory Vlasov–Poisson equations*, *Multiscale Modeling & Simulation*, **15**(2), 723–744 (2017), Publisher: SIAM.
- [14] JR Fernández, Piotr Kalita, Stanislaw Migoórski, M Carmen Muñoz, C Núñez, *Existence and uniqueness results for a kinetic model in bulk-surface surfactant dynamics*, *SIAM Journal on Mathematical Analysis*, **48**(5), 3065–3089 (2016), Publisher: SIAM.
- [15] JR Fernández, MC Muñoz, C Núñez, *A mixed kinetic-diffusion surfactant model for the Henry isotherm*, *Journal of Mathematical Analysis and Applications*, **389**(1), 670–684 (2012), Publisher: Elsevier.
- [16] Alan Gabel, Satya N Majumdar, Nagendra K Panduranga, S Redner, *Can a lamb reach a haven before being eaten by diffusing lions?*, *Journal of Statistical Mechanics: Theory and Experiment*, **2012**(05), P05011 (2012), Publisher: IOP Publishing, DOI: <https://doi.org/10.1088/1742-5468/2012/05/p05011>.
- [17] Sashikumaar Ganesan, Lutz Tobiska, *Arbitrary Lagrangian–Eulerian finite-element method for computation of two-phase flows with soluble surfactants*, *Journal of Computational Physics*, **231**(9), 3685–3702 (2012), Publisher: Elsevier.
- [18] CE Morgan, CJW Breward, Ian M Griffiths, Peter D Howell, *Mathematical modelling of surfactant self-assembly at interfaces*, *SIAM Journal on Applied Mathematics*, **75**(2), 836–860 (2015), Publisher: SIAM.
- [19] G. Oshanin, O. Bénichou, M. Coppey, M. Moreau, *Trapping reactions with randomly moving traps: Exact asymptotic results for compact exploration*, *Phys. Rev. E*, **66**,

- 060101 (2002), Publisher: American Physical Society, DOI: <https://doi.org/10.1103/PhysRevE.66.060101>.
- [20] G. Oshanin, O. Vasilyev, P. L. Krapivsky, J. Klafter, *Survival of an evasive prey, Proceedings of the National Academy of Sciences*, **106**(33), 13696-13701 (2009), Publisher: National Academy of Sciences, DOI: <https://doi.org/10.1073/pnas.0904354106>.
- [21] Mark Sussman, Peter Smereka, Stanley Osher, *A level set approach for computing solutions to incompressible two-phase flow, Journal of Computational physics*, **114**(1), 146–159 (1994), Publisher: Elsevier.
- [22] Anne Pierres, Virginie Monnet-Corti, Anne-Marie Benoliel, Pierre Bongrand, *Do membrane undulations help cells probe the world?, Trends in Cell Biology*, **19**(10), 428–434 (2009), Publisher: Elsevier, DOI: <https://doi.org/10.1016/j.tcb.2009.05.009>.
- [23] Alan A. Berryman, *The Origins and Evolution of Predator-Prey Theory, Ecology*, **73**(5), 1530-1535 (1992), Publisher: Ecological Society of America, DOI: <https://doi.org/10.2307/1940005>
- [24] Antonio Raudino, Antonio Grassi, Giuseppe Lombardo, Giovanni Russo, Clarissa Astuto, Mario Corti, *Anomalous Sorption Kinetics of Self-Interacting Particles by a Spherical Trap, Communications in Computational Physics*, **31**(3), 707–738 (2022), Publisher: Global Science Press, DOI: <https://doi.org/10.4208/cicp.0A-2021-0101>
- [25] A. Raudino, D. Raciti, A. Grassi, M. Pannuzzo, M. Corti, *Oscillations of Bubble Shape Cause Anomalous Surfactant Diffusion: Experiments, Theory, and Simulations, Langmuir*, **32**(44), 1168574–1168583 (2016), DOI: [10.1021/acs.langmuir.6b02054](https://doi.org/10.1021/acs.langmuir.6b02054).
- [26] Kuan Xu, MR Booty, Michael Siegel, *Analytical and computational methods for two-phase flow with soluble surfactant, SIAM Journal on Applied Mathematics*, **73**(1), 523–548 (2013), SIAM.
- [27] M. H. Rahmani Doust and S. GHolizade, *The Lotka-Volterra Predator-Prey Equations, Caspian Journal of Mathematical Sciences (CJMS)*, **3**(2), 221–225, 2014, University of Mazandaran, DOI: https://doi.org/your_doi_here
- [28] Mario Corti, Martina Pannuzzo, and Antonio Raudino, *Out of equilibrium divergence of dissipation in an oscillating bubble coated by surfactants, Langmuir*, **30**(2), 477–487, 2014, ACS Publications
- [29] Mario Corti, Martina Pannuzzo, and Antonio Raudino, *Trapping of sodium dodecyl sulfate at the air–water interface of oscillating bubbles, Langmuir*, **31**(23), 6277–6281, 2015, ACS Publications
- [30] H.C. Berg and E.M. Purcell, *Physics of chemoreception, Biophysical Journal*, 1977, DOI: [https://doi.org/10.1016/0370-1573\(83\)90078-9](https://doi.org/10.1016/0370-1573(83)90078-9)

- [31] Stanley Osher and Ronald Fedkiw, *Level set methods and dynamic implicit surfaces*, *Applied Mathematical Sciences*, **153**, Springer-Verlag, New York, 2003, DOI: <https://doi.org/10.1007/b98879>
- [32] Giovanni Russo and Peter Smereka, *A remark on computing distance functions*, *Journal of Computational Physics*, **163**(1), 51–67, 2000, Elsevier
- [33] J. A. Sethian, *Level set methods and fast marching methods: evolving interfaces in computational geometry, fluid mechanics, computer vision, and materials science*, *Cambridge University Press*, 2nd ed., Cambridge monographs on applied and computational mathematics 3, 1999, <http://gen.lib.rus.ec/book/index.php?md5=84883b1f633449f85363f4df6e4e33f2>